Phonon conduction in silicon nanobeams

Woosung Park, Dongsuk D. Shin, Soo Jin Kim, Joseph S. Katz, Joonsuk Park, Chae Hyuck Ahn, Takashi Kodama, Mehdi Asheghi, Thomas W. Kenny, and Kenneth E. Goodson

Citation: Appl. Phys. Lett. **110**, 213102 (2017);

View online: https://doi.org/10.1063/1.4983790

View Table of Contents: http://aip.scitation.org/toc/apl/110/21

Published by the American Institute of Physics

Phonon conduction in silicon nanobeams

Woosung Park,[1] Dongsuk D. Shin,[1] Soo Jin Kim,[2] Joseph S. Katz,[3] Joonsuk Park,[4] Chae Hyuck Ahn,[1] Takashi Kodama,[1] Mehdi Asheghi,[1] Thomas W. Kenny,[1] and Kenneth E. Goodson[1,a)]
[1]*Department of Mechanical Engineering, Stanford University, Stanford, California 94305, USA*
[2]*Geballe Laboratory for Advanced Materials, Stanford University, Stanford, California 94305, USA*
[3]*Department of Electrical Engineering, Stanford University, Stanford, California 94305, USA*
[4]*Department of Materials Science and Engineering, Stanford University, Stanford, California 94305, USA*

(Received 6 March 2017; accepted 8 May 2017; published online 22 May 2017)

Despite extensive studies on thermal transport in thin silicon films, there has been little work studying the thermal conductivity of single-crystal rectangular, cross-sectional nanobeams that are commonly used in many applications such as nanoelectronics (FinFETs), nano-electromechanical systems, and nanophotonics. Here, we report experimental data on the thermal conductivity of silicon nanobeams of a thickness of ~78 nm and widths of ~65 nm, 170 nm, 270 nm, 470 nm, and 970 nm. The experimental data agree well (within ~9%) with the predictions of a thermal conductivity model that uses a combination of bulk mean free paths obtained from *ab initio* calculations and a suppression function derived from the kinetic theory. This work quantifies the impact of nanobeam aspect ratios on thermal transport and establishes a criterion to differentiate between thin films and beams in studying thermal transport. The thermal conductivity of a 78 nm × 65 nm nanobeam is ~32 $W m^{-1} K^{-1}$, which is roughly a factor of two smaller than that of a 78 nm thick film. *Published by AIP Publishing.* [http://dx.doi.org/10.1063/1.4983790]

Thermal transport plays a critical role in many nanoscale systems such as integrated nanoelectronics,[1–3] nano-electromechanical systems (NEMS),[4–8] and nanophotonics.[9–11] Among various forms of devices, nanobeams with rectangular cross-sections are commonly used in applications such as fin field-effect transistors (FinFETs).[12] The thermal conductivity of nanobeams with cross-sectional dimensions comparable to mean free paths (MFPs) of energy carriers is significantly reduced due to boundary scattering. Previous experimental work has investigated the impact of the phonon-boundary scattering on thermal transport properties in nearly pure silicon nanostructures such as thin films,[13–20] nanowires,[21,22] and films/beams with nanoscale features.[23–28] However, there have been no systematic experiments that quantify the impact of cross-sectional aspect ratio on thermal conductivity in the axial-direction of silicon nanobeams.

The MFPs for bulk materials have been studied using theoretical calculations[29] and novel experiments,[30,31] and the phonon MFP of silicon ranges from ~1 nm to ~10 μm at room temperature.[29] The MFPs are suppressed due to nanoscale features, and the reduction in thermal conductivity is determined through the comparison of the characteristic length of the nanostructure with the bulk MFPs.[31–35] For particular geometries, such as thin films and nanowires, a suppression function is determined analytically by integrating the Boltzmann transport equation with appropriate boundary conditions. Thermal transport along the in-plane direction of thin films is described using the Fuchs-Sondheimer approach,[36,37] where the suppression function depends on the ratio of the characteristic length—thickness—to phonon MFPs.[13] For cylindrical shapes, such as nanowires, an analytical solution of the Boltzmann transport is given by Dingle,[38] with the characteristic length being the diameter. For general structures with a constant cross-section, a suppression function has been derived from the kinetic theory by Chambers, which stands on simplifying the assumptions of the boundary scattering process.[39] While Chamber's model shows the identical mathematical expression for thin films and cylindrical shape wires,[37,39] a suppression function for rectangular beams has not been thoroughly examined. In addition to the lack of experimental thermal conductivity data, the absence of a validated suppression function leads to an incomplete understanding of the impact of the sidewall boundary scattering mechanism.

Here, we present an experimental study of phonon transport in silicon nanobeams with varying cross sectional aspect ratios. The beam width, w, is modulated while maintaining a constant thickness, $t = \sim 78$ nm, to control the impact of phonon scattering at the sidewall boundaries of the beams. The aspect ratio of w to t ranges from ~0.9 to ~12.1, and the beams are 10 μm long to ensure diffusive phonon transport in the axial direction of the beam at room temperature. Specifically, we fabricate five different samples with widths ~65 nm, 170 nm, 270 nm, 470 nm, and 970 nm as shown in Figs. 1(b)–1(f). The range of sample dimensions is designed to capture the transition from a nanobeam with a square cross-section to a thin film. Through a combination of bulk MFPs taken from *ab initio* calculations[29] and a suppression function derived by Chambers,[39] the thermal conductivities of nanobeams are predicted. We explore thermal transport in the transition from nanobeams to thin films. Using the thermal conductivity accumulation function in nanobeams, we investigate the relative contributions of phonons with different MFPs to thermal conductivity.

Patterned nanobeams are stretched between two suspended "hot" and "cold" platforms[21,40] as shown in Fig. 1(a). The samples are fabricated on silicon-on-insulator (SOI)

a)Author to whom correspondence should be addressed: goodson@stanford.edu

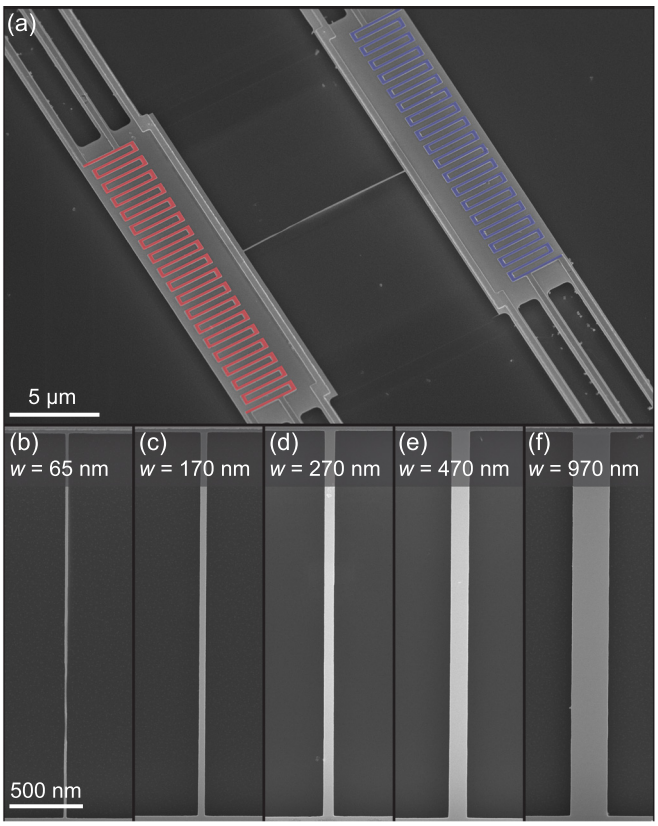

FIG. 1. (a) Overview of the "hot" and "cold" platforms for thermal characterization: false color on heater/thermometers. (b)–(f) Silicon nanobeams, with the width varied from ~65 nm to ~970 nm. The thickness is ~78 nm for all samples.

wafers (Soitec Inc.), which consist of a 340 nm thick silicon device layer and a 1 μm thick buried oxide (BOX) layer. The device layer is boron doped with a resistivity of 14–22 Ω cm and a doping concentration of $\sim 10^{15}$ cm^{-3}, which has a negligible effect on thermal conduction.[41] First, the device layer is thinned down to ~78 nm by thermal oxidation and subsequent removal of the oxide using a wet etching process (6:1 buffered oxide etchant is used). On top of the thinned device layer, ~25 nm thick Al_2O_3 is deposited by atomic layer deposition (ALD) for electrical passivation between metal contacts and the device layer. A 10 μm × 20 μm window is patterned between the two islands by photolithography, and the passivation layer is removed using a combination of reactive ion etching (RIE) and wet etching processes. In this open area, the nanobeams are patterned by electron-beam lithography, and RIE is used to remove the silicon in the non-sample area. The metal heater/thermometer lines on the "hot" and "cold" platforms are patterned by electron-beam lithography, and ~5 nm thick Cr and ~40 nm thick Pt are deposited through electron-beam metal evaporation, followed by a liftoff process. An electrical access, including contact pads and connecting lines to the metal heater/thermometers, is patterned by photolithography, metalized with ~5 nm thick Cr and ~40 nm thick Pt, followed by a liftoff process. The BOX layers in the surrounding area of the islands and legs are etched using RIE, and they are suspended by vapor phase hydrogen fluoride (HF) etching to remove the buried oxide under the sample area. All dimensions are measured by scanning electron microscopy (SEM) after fabrication.

The silicon nanobeams are characterized by electro-thermal characterization that is done for carbon-nanotube and nanowire measurements.[40,42] Heat is generated in the "hot" platform by Joule heating in the serpentine Pt resistor, which is then conducted through the nanobeam test-section to the "cold" platform, and the remaining heat is conducted away via the 6 supporting beams to the chip. Temperatures at the "hot" and "cold" platforms are measured by resistive thermometry and are controlled to maintain a temperature difference to be smaller than ~8 K. The thermal conductance of the nanobeam is measured and used to extract its thermal conductivity for a given nanobeam geometry. All of the measurements are performed under vacuum to eliminate convective heat loss from the platforms and nanobeam. The heat loss through radiation is negligible compared to the thermal conduction path between the "hot" and "cold" platforms. The interfacial resistances between the heater/thermometers and the islands are orders of magnitude smaller than those of the nanobeam test-section, and the interfacial resistance is considered negligible.[43] The experimental uncertainty is primarily attributed to the inaccuracy in sample dimensions, which is inherent in nanofabrication and scanning electron microscopy (SEM) measurements. The measurement error for all samples is estimated to be less than ~9% of the thermal conductivity.

Figure 2 depicts the thermal conductivity of the silicon nanobeam versus width for a thickness of ~78 nm. The thermal conductivity increases monotonically with the increasing beam width, from ~32 to ~51 W m^{-1} K^{-1} when the width w increases from ~65 nm to ~970 nm. The thermal conductivity of the nanobeam with $w = \sim 970$ nm is ~96% of the predicted value of ~53 W m^{-1} K^{-1} for a thickness of 78 nm film. The in-plane thermal conductivity of the 78 nm thick film is estimated using a model described below. The thermal conductivity of the beam with w = ~65 nm drops by ~58% due to the finite width comparable to that of the thin film. The

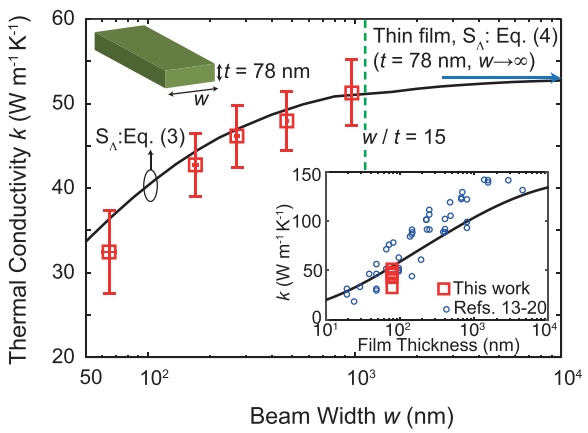

FIG. 2. Thermal conductivity for nanobeams with various aspect ratios, w/t, from ~0.9 to ~12.1. Red hollow squares indicate the experimental values, and the black solid line indicates the model prediction using Eq. (3) for a suppression function. The thickness for beams is fixed to be $t = 78$ nm. The blue solid arrow indicates the cases of thin films, and the value is predicted using Eq. (4) for a suppression function. The green dashed line indicates the case where the aspect ratio $w/t = 15$. The experimental data for this present work are compared with thin films with varying thickness as shown in the inset on the bottom right. The thermal conductivities denoted as blue circles in this inset are obtained from Refs. 13–20, and a black solid line in the inset represents the model prediction calculated using Eq. (4). The interior figure on top left shows the schematic of the cross-section of the nanobeam.

variation in the measured thermal conductivity of the beams shows the relative importance of boundary scattering on sidewall boundaries. Specifically, the thermal conductivity changes most significantly when the width of the beam is comparable to its thickness. This indicates that a significant fraction of MFPs in thin films are concentrated around their thickness.

To investigate the suppression of phonon propagation, we model the thermal conductivity of the silicon nanobeams. The axial thermal conductivity of a beam is[31,34,44]

$$k_{Beam} = \int_0^\infty S_\Lambda(A_C, \Lambda_{bulk}) f(\Lambda_{bulk}) d\Lambda_{bulk}, \tag{1}$$

where S_Λ is the heat flux suppression function, f is the differential MFP distribution for bulk media, A_C is the cross-sectional area, and Λ_{bulk} is phonon MFPs of a bulk medium. The suppression function for a cross-sectional area A_C is obtained by Chambers with diffuse boundary scattering assumptions, and the function is given by[39]

$$S_\Lambda(A_C, \Lambda_{bulk}) = 1 - \frac{3}{4\pi A_C} \int dA_C \int_0^{2\pi} d\varphi \times \int_0^\pi d\theta \sin\theta \cos\theta^2 \exp\left(\frac{-\overline{OP}}{\Lambda_{bulk}}\right), \tag{2}$$

where $\overline{OP}$ is the distance from the surrounding surface to a point inside the structure. For a rectangular cross-section with width w and thickness t, we express the suppression function in a closed form.[45]

$$\begin{aligned} S_{\Lambda,\mathrm{beam}}\left(A_C(w,t), \Lambda_{bulk}\right) = 1 &- \frac{3}{4\pi wt}\int_0^w dx \int_0^t dy \int_{-\tan^{-1}(y/x)}^{\tan^{-1}\left((t-y)/x\right)} d\varphi \int_0^\pi d\theta \left\{ \sin\theta\cos^2\theta \exp\left(\frac{-x}{\Lambda_{bulk}\sin\theta\cos\varphi}\right)\right\} \\ &- \frac{3}{4\pi wt}\int_0^w dx \int_0^t dy \int_{-\tan^{-1}\left(x/(t-y)\right)}^{\tan^{-1}\left((w-x)/(t-y)\right)} d\varphi \int_0^\pi d\theta \left\{ \sin\theta\cos^2\theta \exp\left(\frac{-(t-y)}{\Lambda_{bulk}\sin\theta\cos\varphi}\right)\right\} \\ &- \frac{3}{4\pi wt}\int_0^w dx \int_0^t dy \int_{-\tan^{-1}\left((t-y)/(w-x)\right)}^{\tan^{-1}\left(y/(w-x)\right)} d\varphi \int_0^\pi d\theta \left\{ \sin\theta\cos^2\theta \exp\left(\frac{-(w-x)}{\Lambda_{bulk}\sin\theta\cos\varphi}\right)\right\} \\ &- \frac{3}{4\pi wt}\int_0^w dx \int_0^t dy \int_{-\tan^{-1}\left((w-x)/y\right)}^{\tan^{-1}(x/y)} d\varphi \int_0^\pi d\theta \left\{ \sin\theta\cos^2\theta \exp\left(\frac{-y}{\Lambda_{bulk}\sin\theta\cos\varphi}\right)\right\}. \end{aligned} \tag{3}$$

We use the differential MFP function f from *ab initio* calculations for bulk silicon.[29] Through a combination of the suppression function and the MFP distribution, the thermal conductivity of beams with a rectangular cross-section is predicted as shown in Fig. 2. The largest discrepancy between the model prediction and the experiments is found for the sample with $w = \sim 65$ nm, and the discrepancy is mainly due to potential uncertainty in sample dimensions. The model prediction and the experimental results show close agreement to within ~9%, which is within the error bars of the measurements.

Using the Boltzmann transport model, we explore the transition between beams with a finite aspect ratio and thin films. Liu suggests that for thermal transport, a rectangular cross-section can be considered as a thin film when $w/t > 15$.[45] To examine this criterion, we compare the thermal conductivity of a ~78 nm thick thin film and a ~78 nm thick nanobeam with the increasing aspect ratio. The analytic suppression function for thin films is given by[13,37]

$$S_{\Lambda,thin\,film}(A_C(t), \Lambda_{bulk}) = 1 - \frac{3}{8\xi} + \frac{3}{2\xi}\int_1^\infty \left(\frac{1}{x^3} - \frac{1}{x^5}\right) e^{-\xi} dx, \tag{4}$$

where $\xi = \frac{t}{\Lambda_{bulk}}$. The model using Eq. (4) predicts the thermal conductivity of thin films as shown in the inset of Fig. 2. The predicted thermal conductivity of nanobeams monotonically rises with the increasing width and approaches that of thin films as shown in Fig. 2. When the aspect ratio is 15:1, the thermal conductivity of nanobeams is estimated to be 98% that of thin films. This indicates that it is reasonable to consider a beam with an aspect ratio of higher than 15:1 as a thin film for thermal transport. We note that this criterion is purely based on the aspect ratio of the beams, regardless of the ratio of the characteristic length to the bulk MFPs.

To understand the MFP specific impact of the thickness and width of beams, we calculate a thermal conductivity accumulation, which is given by[44]

$$F(A_C, \Lambda_{bulk}) = \int_0^{\Lambda_{bulk}} S_\Lambda\left(A_C, \Lambda'\right) f(\Lambda') d\Lambda'. \tag{5}$$

We note that the accumulation function is plotted with bulk MFPs. We compare three different cases: bulk silicon, a thin film with $t = \sim 78$ nm, and a beam with $w = t = \sim 78$ nm. For the bulk case, the suppression function is a unity function. The accumulation function shows the relative contribution of a wide range of MFPs to the thermal conductivity. Compared to the bulk material, the accumulation functions for the nanostructures are significantly suppressed as shown in Fig. 3, and such suppression is highlighted for long MFPs compared to its characteristic length, t. Due to the minimal contribution of phonons with long MFPs, the spectrum of MFPs in nanostructures is concentrated near their characteristic length. To quantify the concentration of MFPs, we introduce a concept of a bandwidth using a characteristic

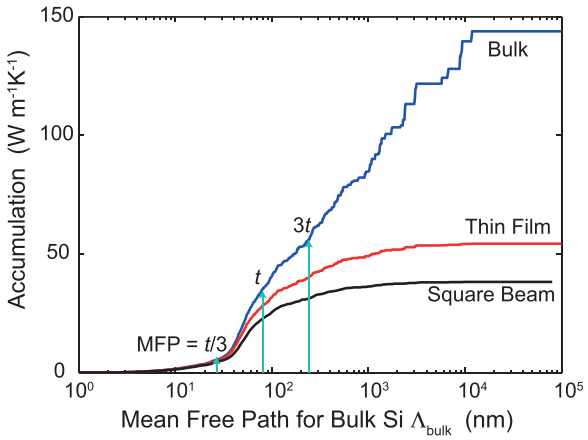

FIG. 3. Accumulation of thermal conductivity with a function of mean free paths for bulk silicon, a thin film with t, and a square beam with $t = w$, where $t = 78$ nm. The accumulation function is calculated using Eqs. (3)–(5).

length, i.e., thickness in this work. The bandwidth is set from a third of the characteristic length, $t/3$, to three times that, $3t$. This bandwidth indicates a transition from a region where internal scattering dominates to the counterpart where boundary scattering becomes predominant. Specifically, while the phonons with the MFPs of the bandwidth contribute to ~35% of the thermal conductivity for bulk silicon, the phonons with the MFPs in this range of the bandwidth contribute to ~64% and ~70% of the thermal conductivity for thin films and square beams, respectively. For short MFPs smaller than $t/3$, MFP distribution does not significantly change, which indicates diffusive phonon transport, following Fourier's law. Since optical phonons have relatively small MFPs, the increased importance of phonons with MFPs below the bandwidth implies that optical phonons become important in axial thermal transport.[46] Phonons with long MFPs are mainly suppressed due to boundary scattering. It is also worth noting that MFPs longer than $3t$ still appreciably contribute to the thermal conductivities of 26% and 18% of the film ($t = 78$ nm) and the rectangular cross sectional ($t = 78$ nm and $w = 78$ nm) nanobeam, respectively. This suggests that controlling long MFPs phonons can be a key to the manipulation of the thermal conductivity of nanostructures.

In this work, we present experimental data of the thermal conductivity of ~78 nm thick silicon nanobeams with various aspect ratios. The combination of MFP distributions for bulk silicon from *ab initio* calculations and the suppression function from the kinetic theory provides a convenient and efficient way to calculate the thermal conductivity of rectangular beam structures. This validated model is particularly relevant for many applications such as microelectromechanical systems and microelectronics, where beam structures are commonly found. We further investigate the thermal conductivity accumulation function for nanobeams and thin films, and the function helps understand which range of MFPs is important for thermal transport.

The authors thank Keivan Esfarjani for sharing his MFP spectra. This work was supported by the National Science Foundation under Grant No. 1336734. The authors acknowledge the use of the Stanford Nano Shared Facilities (SNSF) of Stanford University for sample preparation and characterization.

[1]M. Ieong, B. Doris, J. Kedzierski, K. Rim, and M. Yang, Science **306**(5704), 2057 (2004).
[2]B. Raj, A. Saxena, and S. Dasgupta, IEEE Circuits Devices Mag. **11**(3), 38 (2011).
[3]I. Ferain, C. A. Colinge, and J.-P. Colinge, Nature **479**(7373), 310 (2011).
[4]S. S. Verbridge, H. G. Craighead, and J. M. Parpia, Appl. Phys. Lett. **92**(1), 13112 (2008).
[5]J. S. Bunch, A. M. Van Der Zande, S. S. Verbridge, I. W. Frank, D. M. Tanenbaum, J. M. Parpia, H. G. Craighead, and P. L. McEuen, Science **315**(5811), 490 (2007).
[6]A. H. Safavi-Naeini, J. Chan, J. T. Hill, T. P. M. Alegre, A. Krause, and O. Painter, Phys. Rev. Lett. **108**(3), 033602 (2012).
[7]R. Lifshitz and M. L. Roukes, Phys. Rev. B **61**(8), 5600 (2000).
[8]K. Padmaraju and K. Bergman, Nanophotonics **3**(4–5), 269 (2014).
[9]K.-Y. Jeong, Y.-S. No, Y. Hwang, K. S. Kim, M.-K. Seo, H.-G. Park, and Y.-H. Lee, Nat. Commun. **4**(1), 2822 (2013).
[10]Y. X. Yeng, M. Ghebrebrhan, P. Bermel, W. R. Chan, J. D. Joannopoulos, M. Soljačić, and I. Celanovic, Proc. Natl. Acad. Sci. U.S.A. **109**(7), 2280 (2012).
[11]Y. A. Vlasov, IEEE Commun. Mag. **50**(2), s67 (2012).
[12]D. Hisamoto, L. Wen-Chin, J. Kedzierski, H. Takeuchi, K. Asano, C. Kuo, E. Anderson, K. Tsu-Jae, J. Bokor, and H. Chenming, IEEE Trans. Electron Devices **47**(12), 2320 (2000).
[13]M. Asheghi, M. Touzelbaev, K. Goodson, Y. Leung, and S. Wong, J. Heat Transfer **120**(1), 30 (1998).
[14]Y. Ju and K. Goodson, Appl. Phys. Lett. **74**(20), 3005 (1999).
[15]W. Liu and M. Asheghi, Appl. Phys. Lett. **84**(19), 3819 (2004).
[16]W. Liu and M. Asheghi, J. Appl. Phys. **98**(12), 123523 (2005).
[17]M. S. Aubain and P. R. Bandaru, Appl. Phys. Lett. **97**(25), 253102 (2010).
[18]J. A. Johnson, A. A. Maznev, J. Cuffe, J. K. Eliason, A. J. Minnich, T. Kehoe, C. M. S. Torres, G. Chen, and K. A. Nelson, Phys. Rev. Lett. **110**(2), 025901 (2013).
[19]E. Chávez-Ángel, J. S. Reparaz, J. Gomis-Bresco, M. R. Wagner, J. Cuffe, B. Graczykowski, A. Shchepetov, H. Jiang, M. Prunnila, J. Ahopelto, F. Alzina, and C. M. S. Torres, APL Mater. **2**(1), 012113 (2014).
[20]X. Liu, X. Wu, and T. Ren, Appl. Phys. Lett. **98**(17), 174104 (2011).
[21]D. Li, Y. Wu, P. Kim, L. Shi, P. Yang, and A. Majumdar, Appl. Phys. Lett. **83**(14), 2934 (2003).
[22]R. Chen, A. I. Hochbaum, P. Murphy, J. Moore, P. Yang, and A. Majumdar, Phys. Rev. Lett. **101**(10), 105501 (2008).
[23]J.-K. Yu, S. Mitrovic, D. Tham, J. Varghese, and J. R. Heath, Nat. Nanotechnol. **5**(10), 718 (2010).
[24]J. Lee, W. Lee, G. Wehmeyer, S. Dhuey, D. L. Olynick, S. Cabrini, C. Dames, J. J. Urban, and P. Yang, Nat. Commun. **8**, 14054 (2017).
[25]J. Lim, H.-T. Wang, J. Tang, S. C. Andrews, H. So, J. Lee, D. H. Lee, T. P. Russell, and P. Yang, ACS Nano **10**(1), 124 (2016).
[26]N. Zen, T. A. Puurtinen, T. J. Isotalo, S. Chaudhuri, and I. J. Maasilta, Nat. Commun. **5**, 3435 (2014).
[27]A. M. Marconnet, T. Kodama, M. Asheghi, and K. E. Goodson, Nanoscale Microscale Thermophys. Eng. **16**(4), 199 (2012).
[28]L. Yang, Y. Yang, Q. Zhang, Y. Zhang, Y. Jiang, Z. Guan, M. Gerboth, J. Yang, Y. Chen, and D. G. Walker, Nanoscale **8**(41), 17895 (2016).
[29]K. Esfarjani, G. Chen, and H. T. Stokes, Phys. Rev. B **84**(8), 085204 (2011).
[30]K. T. Regner, D. P. Sellan, Z. Su, C. H. Amon, A. J. McGaughey, and J. A. Malen, Nat. Commun. **4**, 1640 (2013).
[31]A. J. Minnich, Phys. Rev. Lett. **109**(20), 205901 (2012).
[32]Y. Hu, L. Zeng, A. J. Minnich, M. S. Dresselhaus, and G. Chen, Nat. Nanotechnol. **10**(8), 701 (2015).
[33]J. Cuffe, J. K. Eliason, A. A. Maznev, K. C. Collins, J. A. Johnson, A. Shchepetov, M. Prunnila, J. Ahopelto, C. M. Sotomayor Torres, G. Chen, and K. A. Nelson, Phys. Rev. B **91**(24), 245423 (2015).
[34]H. Zhang, C. Hua, D. Ding, and A. J. Minnich, Sci. Rep. **5**, 9121 (2015).
[35]H. Zhang, X. Chen, Y.-D. Jho, and A. J. Minnich, Nano Lett. **16**(3), 1643 (2016).
[36]K. Fuchs, Math. Proc. Camb. Philos. Soc. **34**(01), 100 (1938).
[37]E. H. Sondheimer, Adv. Phys **1**(1), 1 (1952).
[38]R. B. Dingle, Proc. R. Soc. A **201**(1067), 545 (1950).
[39]R. G. Chambers, Proc. R. Soc. A **202**(1070), 378 (1950).

[40]P. Kim, L. Shi, A. Majumdar, and P. L. McEuen, Phys. Rev. Lett. **87**(21), 215502 (2001).
[41]M. Asheghi, K. Kurabayashi, R. Kasnavi, and K. Goodson, J. Appl. Phys. **91**(8), 5079 (2002).
[42]L. Shi, D. Li, C. Yu, W. Jang, D. Kim, Z. Yao, P. Kim, and A. Majumdar, J. Heat Transfer **125**(5), 881 (2003).
[43]K. Hippalgaonkar, B. Huang, R. Chen, K. Sawyer, P. Ercius, and A. Majumdar, Nano Lett. **10**(11), 4341 (2010).
[44]F. Yang and C. Dames, Phys. Rev. B **87**(3), 35437 (2013).
[45]W. Liu, Ph.D. thesis, Carnegie Mellon University, 2005.
[46]Z. Tian, K. Esfarjani, J. Shiomi, A. S. Henry, and G. Chen, Appl. Phys. Lett. **99**(5), 053122 (2011).